

## **FDTD ANALYSIS OF THE DISPERSION CHARACTERISTICS OF THE METAL PBG STRUCTURES**

**Ashutosh\* and P. K. Jain**

Center of Research in Microwave Tubes, Department of Electronics Engineering, Institute of Technology, Banaras Hindu University, Varanasi-221005, India

**Abstract**—Two dimensional metallic photonic band gap (PBG) structures, which have higher power handling capability, have been analyzed for their dispersion characteristics. The analysis has been performed using finite difference time domain (FDTD) method based on the regular orthogonal Yee's cell. A simplified unit cell of triangular lattice PBG structure has been considered for the *TE* and *TM* modes of propagation. The EM field equations in the standard central-difference form have been taken in FDTD method. Bloch's periodic boundary conditions have been used by translating the boundary conditions along the direction of periodicity. For the source excitation, a wideband Gaussian pulse has been used to excite the possible modes in the computational domain. Fourier transform of the probed temporal fields has been calculated which provides the frequency spectrum for a set of wave vectors. The determination of eigenfrequencies from the peaks location in the frequency spectrum has been described. This yields the dispersion diagram which describes the stop and pass bands characteristics. Effort has been made to describe the estimation of defect bands introduced in the PBG structures. Further, the present orthogonal FDTD results obtained have been compared with those obtained by a more involved non-orthogonal FDTD method. The universal global band gap diagrams for the considered metal PBG structure have been obtained by varying the ratio of rod radius to lattice constant for both polarizations and are found identical with those obtained by other reported methods. Convergence of the analysis has been studied to establish the reliability of the method. Usefulness of these plots in designing the devices using 2-D metal PBG structure has also been illustrated.

---

*Received 6 December 2011, Accepted 13 February 2012, Scheduled 22 February 2012*

\* Corresponding author: Ashutosh (asingh.rs.ece@itbhu.ac.in).

## 1. INTRODUCTION

Photonic band gap (PBG) structures have aroused considerable research interest primarily due to their frequency and mode selective properties. These fascinating properties lead improved performances of the PBG based electronic devices, both active as well as passive. Two dimensional (2-D) PBG structures have potential application in microwave, millimeter-wave and infrared devices, which include waveguides, filters, resonators, antennas, planar reflectors, integrated circuits, optical fibers, lasers, etc. [1–3]. PBG structures are also successfully being used in the vacuum electron beam devices, such as, gyrotrons, high gradient accelerators, multibeam reflex klystrons, backwards wave oscillators (BWO) and, traveling wave tubes, etc. [1–3].

PBG structures are lattices of periodic structure utilizing dielectric, metallic or composite inclusions. These periodic structures offer propagation of EM waves in certain frequency band known as the propagating/pass band and no waves exist in the forbidden/stop band, is known as “photonic or electromagnetic band gap”. Dielectric PBG structures have been utilized in various devices for different kind of applications. However, researches in metal photonic band gap (MPBG) structures lead enormous important applications due to their higher power handling capability over its dielectric counterpart. The problem of breakdown and charging of dielectric materials restricts its applications. On the contrary, these phenomena do not happen in the metal due to their excellence conductivity and performs as a nearly perfect reflector at high frequency which also minimizes the problems of absorption [3, 4]. Moreover, in vacuum electronics devices, operating temperature is very high which necessitates the interaction structure’s material to sustain this temperature with sufficient mechanical strength.

Different methods have been applied by researchers in the past to analyze the photonic crystals. These methods include modified plane wave expansion method (PWE) [5], transfer matrix method (TMM) [1, 6], multiple multipole method (MMP) [7], finite-difference frequency-domain (FDFD) method [8], finite element method (FEM) [9] and generalized Rayleigh identity method [10], etc.. The availability of numerous methods for the analysis of PBG structures reflects their wide range of applications and research interest. Some of the methods involves the plasma-like frequency dependence and is not well suited for the calculation of photonic band structure using finite conductivity value such as PWE method. The other methods are cumbersome and more involved than FDTD.

However, the finite difference frequency domain (FDFD) is another counterpart to FDTD for band structure computation but due to some distinct advantages of FDTD, it has been used here.

Finite difference time domain (FDTD) method is a powerful numerical technique widely used by researchers in various fields providing accurate results [11, 12]. The modelling of arbitrarily-shaped structures reinforces the usefulness of FDTD method among wide range of applications. Moreover, with the pulse excitation signal, one can obtain both temporal as well as broadband steady-state response with single calculation. In the non-orthogonal FDTD, the problem of staircase error is reduced, but simultaneously, it requires coordinate transformation and rigorous derivation. The unit cell model taken in the present method overcomes the problem arising due to staircase approximation and can be applied for any dimension of inclusions. Additionally, the conventional FDTD using orthogonal mesh is simpler in implementation as well as involves simpler equations. For most of the other methods, computational time varies with  $N^\alpha$  where,  $\alpha \geq 2$  and  $N$  is number of grid points, but it varies with the  $N$  for FDTD [11]. FDTD using conventional Yee's algorithm requires a high spatial resolution to minimize the numerical dispersion caused by the staircase approximation when curved inclusions/oblique surfaces are involved. For the high spatial resolution case, the requirement of high computational resources can be easily handled with the advent of fast computers having large memories. The material with nonlinear properties can be effectively treated and can be utilized in structures containing dielectric as well as metal [13]. Furthermore, photonic crystal with defects can be suitably realized with no additional computational complication. The non-primitive unit cell of triangular lattice (two circles in one unit cell for 2-D case), can be easily implemented for band structure calculation but this unit cell provides folded version of bands [14]. One should take primitive unit cell to avoid such folded bands.

In the present paper, analysis of the 2-D metal PBG structures, which find applications in high power devices, is presented for dispersion characteristics using FDTD method. Here, a triangular lattice PBG structure with *TE* and *TM* modes of propagation is considered. The analysis of the dielectric PBG structure using modified unit cell technique [14] is extended here for the metal PBG structure. The uniform Yee cell based discretization in orthogonal FDTD method is used for a skew lattice computational domain. The finite conductivity value and permittivity of the metal rod are introduced at the suitable places in the analysis. The implementation of an easy and efficient technique of the translated boundary condition

along the structure periodicity is described. In the present FDTD method, a wideband initial pulse source excitation is incorporated to initialize the computation. The monitoring of the field in time domain and its Fourier transform are described which finally yield the complete dispersion diagram. The dispersion characteristics of the metal PBG structure is further interpreted for obtaining the universal global band gap diagram which exhibits the pass band and stop band needed for designing the devices utilizing these metal PBG crystals. The global band gap diagrams of metal PBG crystal are calculated here for both *TM* and *TE* modes. The band structure obtained here, through the developed FDTD analysis for the metallic PBG structure, is compared and is found identical with those published in the literature though using a more complex and involved non-orthogonal FDTD method [11]. The global band gap diagrams obtained here are also found identical with those obtained using MIT PBGSS code [1].

## 2. PHOTONIC BAND GAP STRUCTURE MODEL

For the analysis, typically, a 2-D metal PBG structure model containing periodic rods in a triangular lattice in *TM* and *TE* modes of propagation is considered. The triangular lattice structure is an azimuthally symmetric and provides more global band gap regions compared to the square lattice for *TE* mode. Dispersion diagram, i.e., band structure is required to determine the forbidden and pass bands of the PBG structures. The lattice, in configuration space and reciprocal space, is shown in Figure 1. The shaded portion shows the irreducible

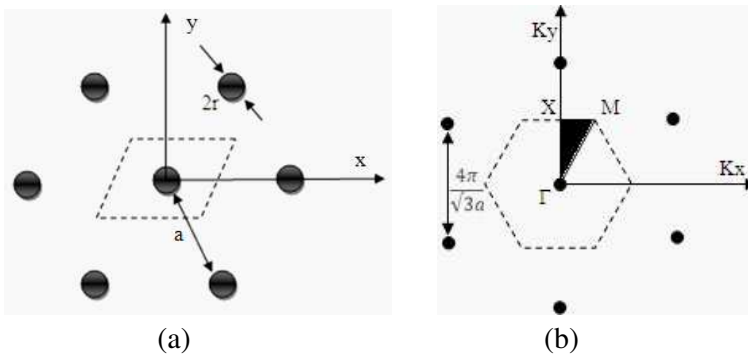


**Figure 1.** Metal PBG structure of triangular lattice, (a) in real space, (b) its reciprocal lattice showing irreducible Brillouin zone by shaded area.

Brillouin zone in which  $\Gamma$ ,  $X$ , and  $M$  are the symmetry points. The calculation of Eigenvalues along the sides ( $\Gamma$ - $X$ ,  $X$ - $M$  and  $M$ - $\Gamma$ ) of Brillouin zone gives the whole frequency spectrum of that lattice with respect to the wave vector, i.e., the dispersion characteristics.

### 3. FINITE DIFFERENCE TIME DOMAIN (FDTD) ANALYSIS

The basic FDTD method involves several initial steps as the spatial definition of the computational domain with an appropriate distribution of physical parameter, appropriate boundary conditions, EM fields calculation at each spatial discretization point and timestep, an excitation source and final post processing to calculate the desired derived results [15]. For the band structure calculation, eigenfrequencies at the symmetry points ( $\Gamma$ ,  $X$ , and  $M$ ) and along the Brillouin zone edges ( $\Gamma$ - $X$ ,  $X$ - $M$  and  $M$ - $\Gamma$ ) of triangular lattice unit cell (Figure 1) are required.

#### 3.1. Unit Cell Discretization

First, the problem space of the finite dimension must be defined for which analysis has to be performed. The problem space needs to be discretized further in accordance with Courant condition [15]. The considered modified unit cell for calculating the band structure is

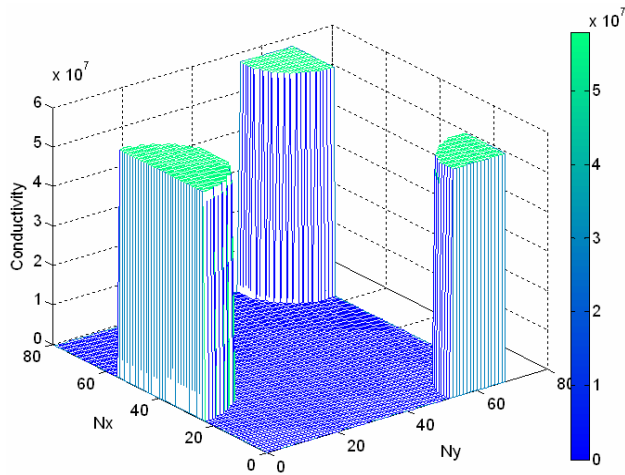


**Figure 2.** Conductivity profile in triangular lattice unit cell for ratio  $r/a = 0.2$ .

discretized into uniform rectangular grids. The length of unit cell along  $y$ -axis is  $\sqrt{3}/2$  times the length along the  $x$ -axis in the unit cell hence if the number of grid points along  $x$ -axis ( $N_x$ ) is 80, then the number of grid points along  $y$ -axis ( $N_y$ ) would be 69, i.e.,  $N_y = \sqrt{3}N_x/2$  (Figure 2).

### 3.2. Material Property Distribution

Now, each grid point must be specified by appropriate material property. Conductivity profile in the unit cell is shown in Figure 2 where half metal cylinders is at middle of one side along  $x$ -direction and two quarter metal cylinder on the other opposite corners. The conductivity ( $\sigma$ ) value is  $5.8 \times 10^7$  S/m for all grid points in metal region with relative permittivity ( $\varepsilon$ ) and relative permeability ( $\mu$ ) as 1. Rest other grid points are assigned with the material property of vacuum ( $\varepsilon$  and  $\mu = 1$ ,  $\sigma = 0$ ).

### 3.3. Time Updating Field Expressions

The time-dependent Maxwell's curl equations are discretized for the rectangular grids. FDTD updating electric ( $E$ ) and magnetic ( $H$ ) field expressions can be derived using time-dependent Maxwell's curl equations, as [15]:

$$\nabla \times \vec{H} = \frac{\partial \vec{D}}{\partial t} + \sigma \vec{E}, \quad \nabla \times \vec{E} = \frac{\partial \vec{B}}{\partial t}.$$

For the 2-D case, in the discretized Maxwell's equations, central difference approximations are used for the space and time derivative of the electric field and magnetic field intensities into two sets of differential equations corresponding to the  $TM$  ( $E$ -polarization) and  $TE$  ( $H$ -polarization) mode. The central difference based discretization used here provides second order accuracy [15]. The above FDTD time updating equations can be written as:

**For TM mode:**

$$\begin{aligned} & E_z^{n+1}\{p, q\} \\ = & \left( \frac{2\varepsilon\{p, q\} - \Delta t\sigma\{p, q\}}{2\varepsilon\{p, q\} + \Delta t\sigma\{p, q\}} \right) \times E_z^n\{p, q\} + \left( \frac{2\Delta t}{2\varepsilon\{p, q\} + \Delta t\sigma\{p, q\}} \right) \\ & \times \left( \frac{H_y^{n+1/2}\{p, q\} - H_y^{n+1/2}\{p-1, q\}}{\Delta x} \right. \\ & \left. - \frac{H_x^{n+1/2}\{p, q\} - H_x^{n+1/2}\{p, q-1\}}{\Delta y} \right) \end{aligned} \quad (1)$$

$$H_x^{n+1/2}\{p, q\} = H_x^{n-1/2}\{p, q\} - \left(\frac{\Delta t}{\mu\{p, q\}}\right) \times \left(\frac{E_z^n\{p, q+1\} - E_z^n\{p, q\}}{\Delta y}\right) \quad (2)$$

$$H_y^{n+1/2}\{p, q\} = H_y^{n-1/2}\{p, q\} + \left(\frac{\Delta t}{\mu\{p, q\}}\right) \times \left(\frac{E_z^n\{p+1, q\} - E_z^n\{p, q\}}{\Delta x}\right) \quad (3)$$

**For TE mode:**

$$\begin{aligned} E_x^{n+1}\{p, q\} &= \left(\frac{2\varepsilon\{p, q\} - \Delta t\sigma\{p, q\}}{2\varepsilon\{p, q\} + \Delta t\sigma\{p, q\}}\right) \times E_x^n\{p, q\} \\ &+ \left(\frac{2\Delta t}{2\varepsilon\{p, q\} + \Delta t\sigma\{p, q\}}\right) \\ &\times \left(\frac{H_z^{n+1/2}\{p, q\} - H_z^{n+1/2}\{p, q-1\}}{\Delta y}\right) \end{aligned} \quad (4)$$

$$\begin{aligned} E_y^{n+1}\{p, q\} &= \left(\frac{2\varepsilon\{p, q\} - \Delta t\sigma\{p, q\}}{2\varepsilon\{p, q\} + \Delta t\sigma\{p, q\}}\right) \times E_y^n\{p, q\} \\ &- \left(\frac{2\Delta t}{2\varepsilon\{p, q\} + \Delta t\sigma\{p, q\}}\right) \\ &\times \left(\frac{H_z^{n+1/2}\{p, q\} - H_z^{n+1/2}\{p-1, q\}}{\Delta x}\right) \end{aligned} \quad (5)$$

$$\begin{aligned} H_z^{n+1/2}\{p, q\} &= H_z^{n-1/2}\{p, q\} + \left(\frac{\Delta t}{\mu\{p, q\}}\right) \\ &\times \left(\frac{E_x^n\{p, q+1\} - E_x^n\{p, q\}}{\Delta y}\right) \\ &- \left(\frac{E_y^n\{p+1, q\} - E_y^n\{p, q\}}{\Delta x}\right) \end{aligned} \quad (6)$$

Here,  $\varepsilon$  and  $\mu$  are the permittivity and permeability of the medium which do not vary with the direction and hence no suffix is provided.  $p$  and  $q$  are the index of grid point in the discretized space and defined as  $\{p, q\} = \{p\Delta x, q\Delta y\}$ , where  $\Delta x$  and  $\Delta y$  are the length of each discretized cell in  $x$  and  $y$  direction. The time  $t$  is also discretized with time increment  $\Delta t$ .  $n$  is an integer denoting time instant. The time evolution of the fields is obtained by these time-stepping equations with a specified source excitation in the computation domain.

### 3.4. Numerical Stability (Courant Criterion)

The electric and magnetic fields are sampled at discrete points both in time as well as space. Sampling period is selected with certain

restriction in such a way that it provides stability in solution. The choice of time step with the space resolution leads the accuracy of results and it is chosen in specific way to obtain the real frequency solution which can be given by Courant-Friedrichs-Lewy (CFL) condition as [15]:

$$\Delta t \leq \Delta t_{\max} = (1/\Delta x^2 + 1/\Delta y^2)^{-1/2}/c \quad (7)$$

where,  $c$  is the velocity of light.  $\Delta x$  and  $\Delta y$  are the controlling factor to have maximum allowed timestep. The timestep must be always smaller than the maximum time step.

### 3.5. Source Excitation or Initial Field Distribution

To start the simulation, a non-zero projection is required which can be provided by a source excitation or an initial field distribution. A modulated Gaussian pulse is taken here since it is very efficient in time-frequency resolution (Figure 3). The important feature of this type of signal is to provide a wideband excitation which requires exciting all possible modes in the unit cell.

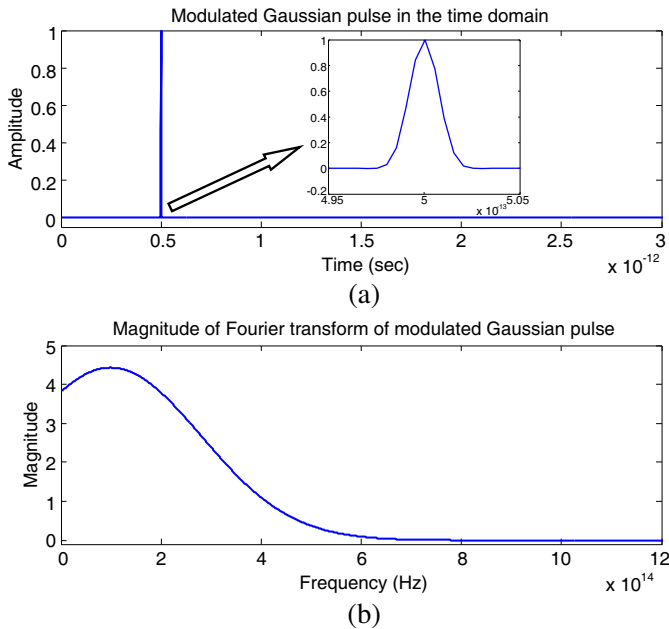


**Figure 3.** The modulated Gaussian pulse as excitation in (a) time domain and (b) frequency domain.

The waveform of the modulated Gaussian pulse can be given as:

$$S\{t\} = A_m e^{j2\pi f t} \exp \left[ -((t - t_0)/\tau)^2 \right] \quad (8)$$

where  $A_m$  is the amplitude of the signal,  $\tau$  is a parameter that determines the width of the Gaussian pulse both in time and frequency domain,  $t_0$  is the amount of time shift and  $f$  is the operating frequency. Here,  $A_m = 1$ ,  $\tau = 1/(8 \times f)$ ,  $f = 10^{14}$  Hz,  $t_0 = 0.5 \times 10^{-12}$  second is taken. In the Gaussian pulse, more energy is concentrated near the center time of the pulse and center frequency. The source excitation should be positioned at several discretization points to excite all possible modes. Only the mode supporting to the structure with the Bloch boundary condition will sustain with the time and all others will vanish. For the band structure calculation, initial field distribution can also be used instead of source excitation with no difference in the final results. The final band structure has no signature of its previous history whether it was a well specified field distribution or excited with a wideband pulse.

### 3.6. Boundary Condition in Unit Cell of Triangular Lattice

Fields at the boundary require satisfying the Bloch boundary condition which can be given as:

$$E(r) = e^{jk \cdot r} e(r), \quad H(r) = e^{jk \cdot r} h(r) \quad (9)$$

$$E(r + a) = e^{jk \cdot a} E(r), \quad H(r + a) = e^{jk \cdot a} H(r) \quad (10)$$

where  $a$  is lattice constant or translational vector.

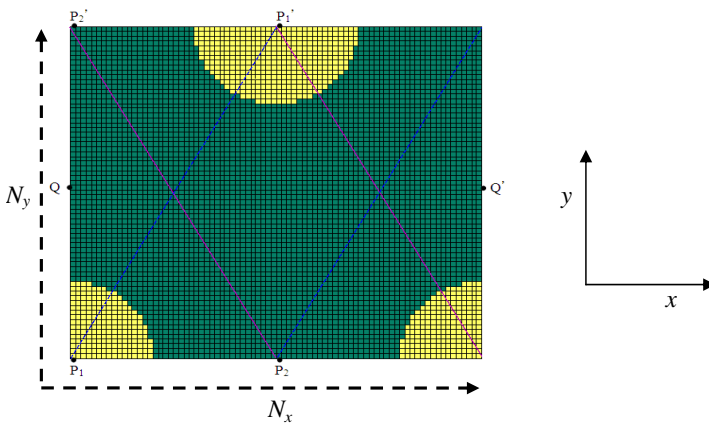


**Figure 4.** Uniformly discretized unit cell of triangular lattice of 2-D metal PBG for  $r/a$  ratio = 0.2.

The scheme of boundary condition implementation along the periodicity is depicted in Figure 4. Boundary condition along the  $x$ -axis ( $p = 0$  to  $N_x$ ) for all grid points is straightforward and this is obtained by translating by  $a$  and can be given as  $Q' = Q \times \exp(-jak_x)$  where  $Q'$  is the grid point at  $p = N_x$  and  $Q$  is at  $p = 0$ . The boundary condition along the  $y$ -axis is divided into two equal parts. First, translating the first half of the horizontal side at bottom side ( $q = 0$ ) by  $a/2$  in positive  $x$ -axis and  $\sqrt{3}a/2$  along positive  $y$ -direction and can be given as:

$$\begin{aligned} P'_1 &= P_1 \times \exp \left[ -ja \left( k_x + \sqrt{3}k_y \right) / 2 \right] \\ P_1 &= P'_1 \times \exp \left[ ja \left( k_x + \sqrt{3}k_y \right) / 2 \right] \end{aligned} \quad (11)$$

Second half of the horizontal bottom side is translated by  $a/2$  in negative  $x$ -direction and  $\sqrt{3}a/2$  in positive  $y$ -direction which can be given as:

$$\begin{aligned} P'_2 &= P_2 \times \exp \left[ -ja \left( -k_x + \sqrt{3}k_y \right) / 2 \right] \\ P_2 &= P'_2 \times \exp \left[ ja \left( -k_x + \sqrt{3}k_y \right) / 2 \right] \end{aligned} \quad (12)$$

So, the field component along  $y$ -axis using Bloch condition can be implemented for computation for all the grid points in following manner,

$$\begin{aligned} &U \left( q = N_y \& p = 0, 1, 2, \dots, \frac{N_x}{2} - 1 \right) \\ &= U \left( q = 0 \& p = \frac{N_x}{2}, \frac{N_x}{2} + 1, \frac{N_x}{2} + 2, \dots, N_x \right) \\ &\quad \times \exp \left[ -ja \left( -k_x + \sqrt{3}k_y \right) / 2 \right] \end{aligned} \quad (13)$$

$$\begin{aligned} &U \left( q = N_y \& p = \frac{N_x}{2}, \frac{N_x}{2} + 1, \frac{N_x}{2} + 2, \dots, N_x \right) \\ &= U \left( q = 0 \& p = 0, 1, 2, \dots, \frac{N_x}{2} - 1 \right) \\ &\quad \times \exp \left[ -ja \left( k_x + \sqrt{3}k_y \right) / 2 \right] \end{aligned} \quad (14)$$

and its inverse can also be derived and used. It should be noticed that for the present analysis, the number of cells must be even otherwise for the odd number of cells, there will be unequal distribution of cells in the unit cell and this will significantly affect the results.

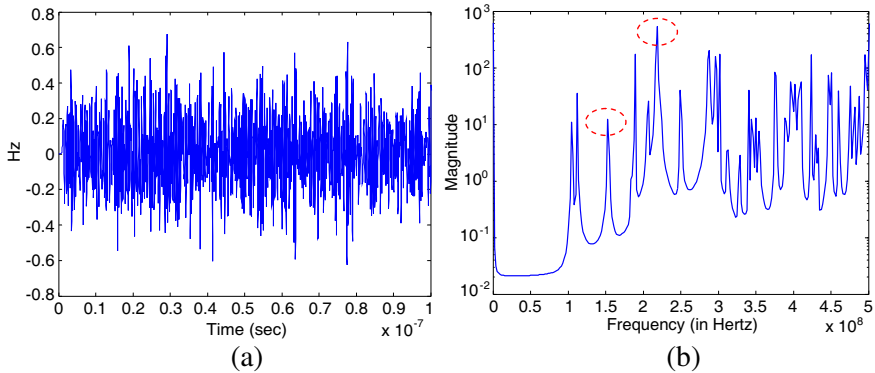


**Figure 5.** (a) Temporal response of  $z$ -component of magnetic field ( $H_z$ ) and (b) its Fourier transform at  $\Gamma$ -point for  $r/a$  equal to 0.2 in  $TE$  mode.

### 3.7. Frequency Domain Transformation and Determination of Frequency Eigenvalue

As the FDTD evolves with time, only the modes satisfying the Bloch boundary condition will remain in the computational domain and other pseudo transmission modes will vanish eventually. The field values at several arbitrary discretization points in the unit cell are recorded to detect all the possible propagating modes. For the  $TE$  case, the recorded  $H_z$  field at gamma point is shown in Figure 5(a). Figure 5(b) demonstrates Fourier transform of the temporal field  $H_z$ . In the figure, there are several peaks obtained at particular definite frequency. These peaks provide the information about the eigenfrequencies (circles in Figure 5(b)), i.e., the peaks of the spectral distribution correspond to the locations of the eigenfrequencies. One must notice that only the location of the spectral peaks is of importance not the shape. This process is done iteratively for all set of wave vectors. Finally, keeping these results together yield the dispersion diagram.

### 3.8. Defect Modes in 2-D PBG Structure

The eigenfrequencies and the field pattern in a lattice with defect can easily be calculated by present FDTD method. A defect in a 2-D PBG lattice can be introduced by removing one or several unit cells of inclusions which leads to localized point or line defect (Figure 6). Defects can also be created by replacing the inclusions with other materials or by changing its shape [16]. For the calculation of defect modes, a supercell (including defect) structure can be considered. The defect band using orthogonal FDTD method can be estimated as the following.

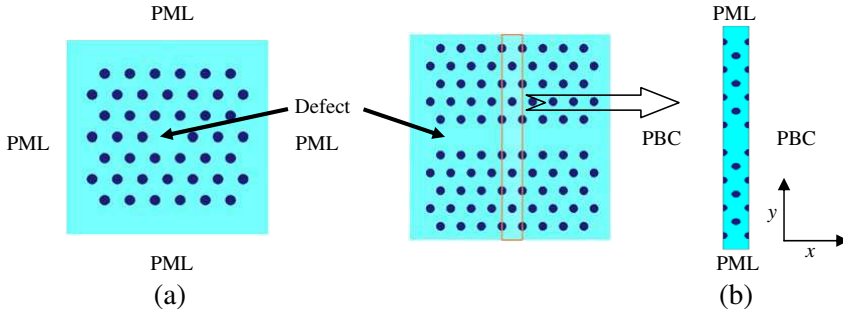


**Figure 6.** Implementation of boundary conditions in the supercell structures of triangular lattice with (a) point and, (b) line defect.

### 3.8.1. Point Defect

Supercell structure with point defect is shown in Figure 6(a) which contains many unit cells of triangular lattice along  $x$ - and  $y$ -direction. The whole computation domain is discretized suitably using Courant criteria (Equation (7)) and it is surrounded by a PML with thickness corresponding to sufficient layers of the discretization grid [15]. Appropriate material property should be assigned for each grid points according to the metal, dielectric or vacuum. The time step with the space resolution is chosen in similar way as for band structure calculation satisfying Courant condition (Equation (7)). FDTD time updating electric ( $E$ ) and magnetic ( $H$ ) field expressions described in Section 3.3 is used. For the excitation in the computational domain, an appropriate wideband signal or an initial field distribution can be used. For initial field case, the initial field should be smooth and continuous in the whole computation space, low symmetry in order to excite all possible defect modes and almost zero outside the defect region. For the boundary condition to this finite sized computational domain of supercell, we use the perfectly matched layer (PML). PML is a finite thickness medium surrounding the computational space to create a wave-impedance matching condition which is independent of angle and frequencies of the wave incident on this boundary. The implementation of the fields inside the PML can be performed using the same FDTD technique [15]. With the time evolution, ultimately the defect modes will exist in the computational domain and other modes will die out. The temporal response of the field is probed in the defect at several points in the computational space and for the spectral information; Fourier transform of the field is calculated. The peaks of the spectral intensity correspond to the locations of the eigenfrequencies of the defect modes. This yields the eigenfrequencies of defect modes for a particular defect region.

### 3.8.2. Line Defect

Line defects in a lattice act as waveguide and most of the steps are similar to that adopted in point defect case for defect bands calculation. Here, differences include the choice of supercell structure and boundary conditions implementation. A supercell is chosen much larger than unit cell containing the waveguide at the center as a computational domain (Figure 6(b)). The length of supercell along  $x$ -direction is chosen equal to the lattice constant value while in  $y$ -direction supercell is chosen more than 10 times of periodicity. Since, the structure is periodic in  $x$ -direction; the periodic boundary condition (PBC) should be assigned and in  $y$ -direction, the computation domain is surrounded with perfectly matched layers (PML) [15]. With the time evolution, only the proper guided modes sustain in the computation space, and other modes will vanish. Similar to the procedure adopted in case of point defect, eigenfrequencies of defect modes can be determined. For  $\Gamma$ - $M$  direction (Figure 1(b)), wave vector is varied and eigenfrequencies of defect modes are recorded which finally yields the defect bands. Even or odd guided modes can be characterized by the symmetry of electric field with respect to the central waveguide plane [16].

## 4. RESULTS AND DISCUSSION

### 4.1. Photonic Band Structure

In the band structure calculation, large numbers of iterations ( $2^{14}$  are sufficient enough) are taken to obtain sufficient accurate results. Sufficient numbers of field probes located at arbitrary grid points in unit cell are used to record all the possible eigenmodes.

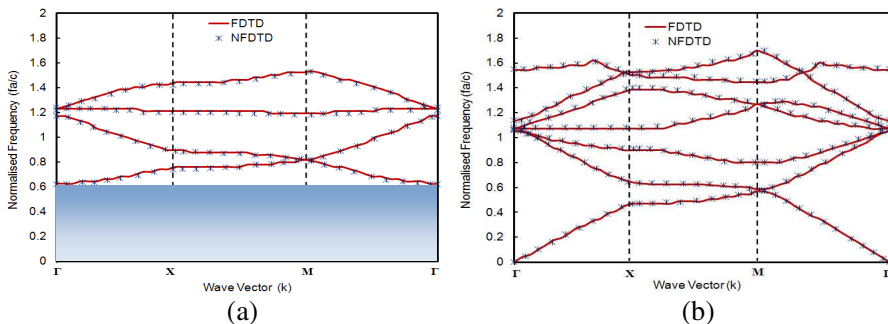


**Figure 7.** Band structure of the 2-D metallic triangular lattice for ratio  $r/a$  is 0.2 for (a)  $TM$  and (b)  $TE$  mode. Shaded portion shows global band gap region.

For the metal PBG structure with triangular lattice operating in the  $TM$  and  $TE$  modes of propagation, the obtained dispersion diagrams using the developed FDTD technique are shown in Figure 7 for the ratio  $r/a$  is 0.2. The vertical axis shows the normalized frequency ( $fa/c$ ) and horizontal axis is wave vector ( $k$ ). Here, only few lowest eigenmodes are shown, though there exist more bands. The band structures are in good agreement with those obtained through non-orthogonal (NFDTD) analysis by Qiu et al. [11]. Obviously, in case of  $TM$  mode, there is a complete band gap, i.e., zeroth order band gap starting from zero frequency and upto a certain frequency or cut-off frequency ((Figure 7(a)) Shaded portion). Moreover, other higher order band gaps are also obtained. For  $TE$  mode (Figure 7(b)), no such zeroth order band gap exists and for this  $r/a$  value (0.2), no global band gaps are observed. For other values of  $r/a$ , there may exist global band gap. For a range of  $r/a$ , the global band gap regions are calculated in next section for  $TM$  and  $TE$  modes.

#### 4.2. Calculation of Global Band Gap Diagram

Now, the global band gap diagrams for the considered metallic PBG structure are calculated using dispersion diagram by varying  $r/a$  for both polarization (Figures 8(a) and 8(b)). In  $TM$  mode global band gap diagram (Figure 8(a)), the region right hand side to the diagram is global band gap region and in the left side is pass band.  $TE$  mode global band gap is shown in Figure 8(b), which consists several global band gap regions. No global band gap occurs before  $r/a$  equal to 0.2. The lowest global band gap occurs between the second and third modes of the dispersion diagram which occurs at  $r/a \geq 0.35$ . The second global  $TE$  band gap occurs between the third and fourth modes

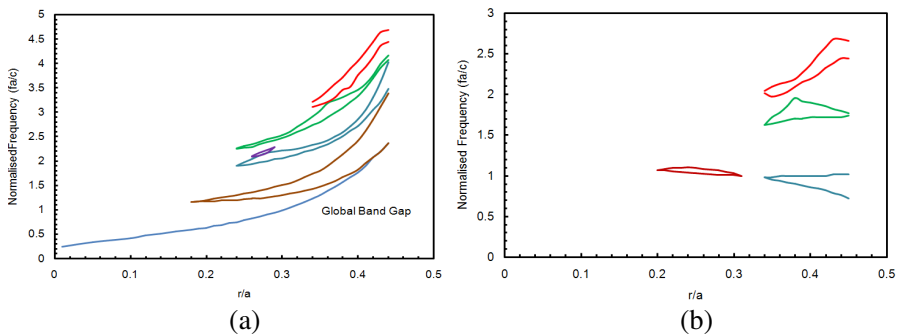


**Figure 8.** Global band gap diagram obtained for the triangular lattice of metal PBG structure in (a)  $TM$  and (b)  $TE$  mode of propagation.

at lower ratios of  $r/a$  than those for the lowest global  $TE$  band gap. Some other global band gaps between higher order modes are also observed as depicted in the figure (normalized frequency  $\geq 2$ ). This global band gap of higher normalized frequency can be used to design the PBG cavity operating in a higher order mode. This global band gap diagram is identical with that obtained using MIT PBGSS code reported by Smirnova et al. [1]. For the single mode of operation of the PBG based waveguide or cavity, the dimension of PBG structure is taken in such a way that the operating frequency of the desired mode must be within the global band gap and that of for all other modes in the pass band.

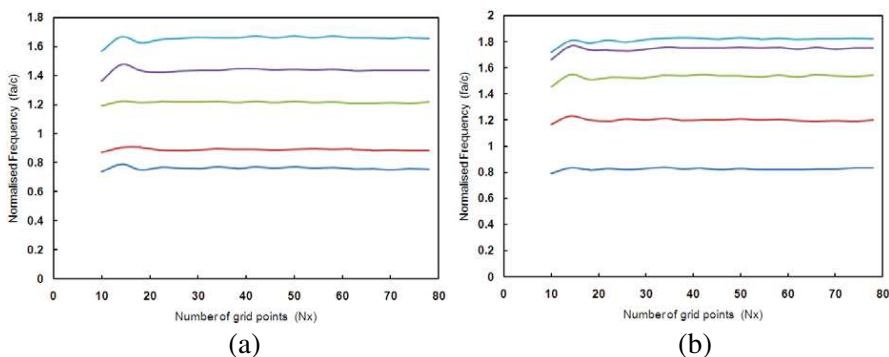


**Figure 9.** The convergence of frequency for  $TM$  mode with  $r/a = 0.2$  at (a)  $X$  and (b)  $M$  symmetry point.

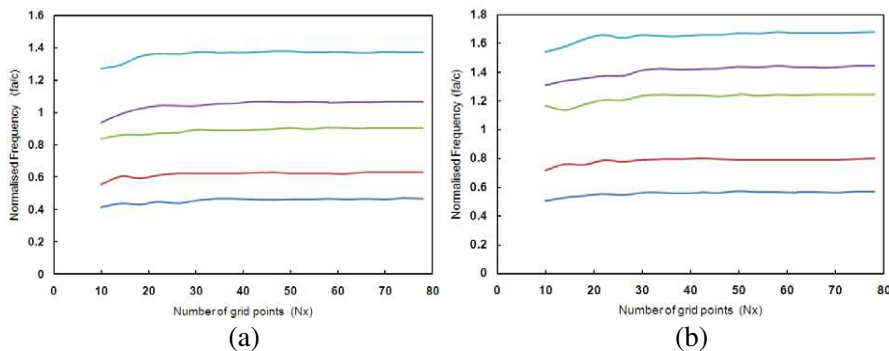


**Figure 10.** The convergence of frequency for  $TE$  mode with for  $r/a = 0.2$  at (a)  $X$  and (b)  $M$  symmetry point.

### 4.3. Convergence Analysis

Convergence is an important aspect of the numerical analysis. Figures 9 and 10 demonstrate the stability and accuracy of the results. The convergence analysis of frequency for  $r/a = 0.2$  and for  $TM$  and  $TE$  mode is performed. First five bands are considered at  $X$  and  $M$  symmetric points and their variation is observed with the number of cells  $N_x$  (and  $N_y = \sqrt{3}N_x/2$ ). For the number of grid points per lattice  $N_x \geq 20$ , this method shows good convergence.

## 5. CONCLUSION

A two dimensional metal photonic band gap structure of triangular lattice has been analyzed for its dispersion characteristics in both  $TE$  and  $TM$  mode of propagation due to its mode selective property. Metal PBG structure has been chosen here for the analysis due to its higher power handling capability over its dielectric counterpart. The triangular lattice of metallic cylindrical rods in the background of vacuum has been selected since this lattice provides better azimuthal symmetry than square lattice. For metal PBG structure analysis, FDTD method has been used which is less cumbersome and easy to implement. The uniform Yee cell based discretization has been used. The steps involved in calculating band structure have been illustrated. A simplified model of primitive unit cell of triangular lattice has been considered in the analysis. This unit cell yields the accurate band structure not the folded bands. The implementation of periodic boundary condition over the unit cell has been presented which is always valid for any computing environment dimension. Staircase error can be reduced using large number of mesh grids in the present FDTD method and therefore large number of mesh grids have been used. In the considered unit cell computational domain, it is easy to incorporate the initial field distribution or point excitation source. A wideband Gaussian source has been used in our approach. The procedure of eigenfrequencies determination from the frequency spectrum of time monitored field has been demonstrated. Photonic band structure obtained from FDTD is compared with the non-orthogonal method and is found in close agreement. The usefulness of universal global band gap curves in the photonic crystal device for  $TM$  and  $TE$  modes has been discussed. Effort is made to describe the estimation of defect bands introduced in the PBG structures. Convergence of the present analysis is also performed and found that sufficient numbers of mesh cells are required for good convergence. Our approach provides good convergence with accurate results. It is hoped that the present dispersion study of the metal PBG structure would be useful for the

designing of the high power devices incorporating PBG structures as its RF propagating structures.

## ACKNOWLEDGMENT

One of the authors (Ashutosh) is thankful to Centre of Advanced Studies (University Grant Commission), Department of Electronics Engineering, IT-BHU, for financial support.

## REFERENCES

1. Smirnova, E. I., C. Chen, M. A. Shapiro, J. R. Sirigiri, and R. J. Temkin, "Simulation of photonic band gaps in metal rod lattices for microwave applications," *J. Appl. Phys.*, Vol. 91, No. 3, 960–968, Feb. 2002.
2. Sirigiri, J. R., K. E. Kreischer, J. Macuhzak, I. Mastovsky, M. A. Shapiro, and R. J. Temkin, "Photonic band gap resonator gyrotron," *Phys. Rev. Lett.*, Vol. 86, 5628–5631, 2001.
3. Gao, X., Z. Yang, Y. Xu, L. Qi, D. Li, Z. Shi, F. Lan, and Z. Liang, "Dispersion characteristic of a slow wave structure with metal photonic band gap cells," *Nuclear Instruments and Methods in Physics Research A*, Vol. 592, 292–296, May 2008.
4. McCalmont, J. S., M. M. Sigalas, G. Tuttle, K. M. Ho, and C. M. Soukolis, "A layer-by-layer metallic photonic band-gap structure," *Appl. Phys. Lett.*, Vol. 68, 2759–2761, 1996.
5. Kuzmiak, V., A. A. Maradudin, and F. Pincemin, "Photonic band structures of two-dimensional systems containing metallic components," *Phys. Rev. B*, Vol. 50, 16835–16844, Dec. 1994.
6. Pendry, J. B. and A. MacKinnon, "Calculation of photon dispersion relations," *Phys. Rev. Lett.*, Vol. 69, No. 19, 2772–2775, Nov. 1992.
7. Moreno, E., D. Erni, and C. Hafner, "Band structure computations of metallic photonic crystals with the multiple multipole method," *Phys. Rev. B*, Vol. 59, No. 3, 1874–1877, Jan. 1999.
8. Guo, S., F. Wu, S. Albin, and R. S. Rogowski, "Photonic band gap analysis using finite difference frequency-domain method," *Optics Express*, Vol. 12, No. 8, 1741–1746, 2004.
9. Hiett, B. P., J. M. Generowicz, S. J. Cox, M. Molinari, D. H. Beckett, and K. S. Thomas, "Application of finite element methods to photonic crystal modeling," *IEE Proceedings Science, Measurement & Technology*, Vol. 149, No. 5, 293–296, Sep. 2005.

10. Nicorovici, N. A., R. C. McPhedran, and L. C. Botten, "Photonic band gaps for arrays of perfectly conducting cylinders," *Phys. Rev. E*, Vol. 52, No. 1, 1135–1145, Jul. 1995.
11. Qiu, M. and S. He, "A nonorthogonal finite-difference time-domain method for computing the band structure of a two-dimensional photonic crystal with dielectric and metallic inclusion," *J. Appl. Phys.*, Vol. 87, No. 12, 8268–8275, Jun. 2000.
12. Kuang, W., W. J. Kim, and J. D. O'Brien, "Finite-difference time domain method for nonorthogonal unit-cell two-dimensional photonic crystals," *Journal of Lightwave Technology*, Vol. 25, No. 9, 2612–2617, Sep. 2007.
13. Arriaga, J., A. J. Ward, and J. B. Pendry, "Order- $N$  photonic band structures for metals and other dispersive materials," *Phys. Rev. B*, Vol. 65, 155120, Apr. 2002.
14. Umenyi, A. V., K. Miura, and O. Hanaizumi, "Modified finite-difference time-domain method for triangular lattice photonic crystals," *Journal of Lightwave Technology*, Vol. 27, No. 22, 4995–5001, Nov. 2009.
15. Elsherbeni, A. Z. and V. Demir, *The Finite Difference Time Domain Method for Electromagnetics with MATLAB Simulations*, Scitech Publishing Inc., Raleigh, 2009.
16. Qiu, M. and S. He, "Guided modes in a two-dimensional metallic photonic crystal waveguide," *Phys. Lett. A*, Vol. 266, 425–429, Feb. 2000.